Extended State Observer Based Sliding Mode Control for Three-Phase Power Converters

Jianxing Liu, *Member*, *IEEE*, Sergio Vazquez, *Senior Member*, *IEEE*, Ligang Wu, *Senior Member*, *IEEE*, Abraham Marquez, *Member*, *IEEE*, Huijun Gao, *Fellow*, *IEEE* and Leopoldo G. Franquelo, *Fellow*, *IEEE*

***Abstract*—This paper proposes an extended state observer based second order sliding mode (SOSM) control for three-phase two-level grid-connected power converters. The proposed control technique forces the input currents to track the desired values, which can indirectly regulate the output voltage while achieving a user-defined power factor. The presented approach has two control loops. A current control loop based on a SOSM and a dc-link voltage regulation loop which consists of an extended state observer (ESO) plus SOSM. In this work, the load connected to the dc-link capacitor is considered as an external disturbance. An ESO is used to asymptotically reject this external disturbance. Therefore, its design is considered in the control law derivation to achieve high performance. Theoretical analysis is given to show the closed-loop behavior of the proposed controller and experimental results are presented to validate the control algorithm under a real power converter prototype.**

***Index Terms*—Sliding mode control, extended state observer, power factor correction, three-phase power converters.**

I. Introduction

THREE-phase pulse-width-modulated (PWM) converters play a key role in industrial applications like integration of renewable energy sources, energy storage systems, motor drives, etc [1]–[5]. Particularly, active front ends (AFE) are grid-connected converters that offer features as bidirectional power flow, near-sinusoidal currents, and power factor and dc-link capacitor voltage regulation capability [6]. For this reason, the control objectives for this application are to maintain the dc-link voltage regulated to a certain reference, supply a desired reactive power and draw grid currents with the lowest possible harmonic distortion.

Manuscript received October 29, 2015; revised April 17, 2016 and July 04, 2016; accepted August 02, 2016. This work was supported by the Ministerio Español de Economia y Competitividad under project ENE2013-45948-R, the Consejeria de Innovacion Ciencia y Empresa (Junta de Andalucia) under the project P11-TIC-7070, the National Natural Science Foundation of China (61525303 and 61503099), the Top-Notch Young Talents Program of China (Ligang Wu) and the China Postdoctoral Science Foundation funded project (2015M570293 and 2016T90291).

S. Vazquez and A. Marquez are with the Electronic Engineering Department, Universidad de Sevilla (Spain), (e-mail: sergi@us.es).

L. G. Franquelo is with the Electronic Engineering Department, Universidad de Sevilla (Spain) and Research Institute of Intelligent Control and Systems, Harbin Institute of Technology, Harbin, 150001, P. R. China (e-mail: lgfranquelo@ieee.org).

J. Liu, L. Wu, and H. Gao are with Research Institute of Intelligent Control and Systems, Harbin Institute of Technology, Harbin, 150001, P. R. China, (e-mail: jx.liu@hit.edu.cn).

There are many approaches to develop the control law for this system. Early solutions were linear regulators like the one proposed in [7]. It changes the modulation index slowly to regulate the dc-link capacitor voltage. Therefore, its main disadvantage is that it presents a slow dynamical response. A faster response can be obtained using a deadbeat current control [8]. However, it is well known that it is highly sensitive to the parameter uncertainties. In general, these approaches define an operating point and then work with a small-signal linearized model around it. This is a drawback because they can not guarantee stability against large signal disturbances for the large range of operating conditions of the three-phase PWM converter due to the fact that AFE are nonlinear systems. Furthermore, the controller implementation requires the system parameters which depend on the operating points, otherwise it may result in steady state errors in the state variables. On the other hand, in light of the strong nonlinearity of AFE, nonlinear control algorithms may be suitable for controlling the power converters, which are able to accommodate a wide range of operating conditions. The main reason is that there's no need to have a linear model of the power converter for nonlinear controller design.

Several nonlinear control approaches have been proposed for grid-tied power converters, such as nonlinear adaptive control [9], passivity based control [10], model predictive control [11] and sliding mode control (SMC) [12]–[16]. Among these techniques, SMC is suitable for dealing with the nonlinear behavior of the considered system due to its characteristics of insensitivity to external disturbances, system reduction, high accuracy and finite time convergence [17], [18].

SMC has been developed as a new control design method for a wide spectrum of systems including nonlinear, time-varying and fault tolerant systems [19]–[21]. SMC can manage the nonlinear behavior of the three-phase grid-connected power converter. Besides, it is characterized to be a robust and effective control strategy. However, up to authors knowledge, proposed SMC strategies have only considered the control of input current in sliding mode [13]–[16]. In general, these works use a proportional integral (PI) controller for the dc-link capacitor voltage regulation. This approach achieves robustness of input current control, but can't guarantee robustness of output voltage control since they are derived using approximations and linearizations. To solve this issue, extended state observer (ESO) based control strategies are proposed for voltage control design to reject disturbances and uncertainties [22], [23]. ESO is an efficient technique for

disturbance estimation, which regards the lumped disturbances (such as parametric uncertainty, unmodeled dynamics and load variation) as a new state. However, only simulation results are provided in both works and stability analysis of the closed loop system taking into account the modelling uncertainties is not performed.

In this paper, a model-based second order sliding mode (SOSM) control for three-phase grid-connected power converters is proposed. The controller design is based on the system model and has a cascaded structure which consists of two control loops. The outer loop regulates the dc-link capacitor voltage and the power factor providing the current references for the inner control loop. The current control loop tracks the actual currents to their desired values.

To design the proposed controller, the load connected to the dc-link capacitor is considered as a disturbance, which directly affects the performance of the whole system. Thus, a composite control law consisting of SOSM based on super-twisting algorithm (STA) and disturbance compensation via ESO is developed for the voltage regulation loop. The current control loop is also designed using the STA. The STA is one of the most popular SOSM algorithms and a unique absolutely continuous sliding mode algorithm, ensuring all the main properties of first order SMC for systems with Lipschitz continuous matched uncertainties/disturbances with bounded gradients [24].

Compared to [22], this paper incorporates the modelling uncertainties into the design of ESO and SOSM algorithms. The sliding surface is designed ensuring the finite time asymptotic convergence of the sliding variables to its desired values in the presence of parametric uncertainties. In addition, this paper provides theoretical study of the stability issue and solves it by Lyapunov method.

To show the benefits of the proposed controller it can be compared with some conventional control strategies like PI synchronous reference frame (PI-SRF) or proportional plus resonant (PR) controllers. The PI-SRF is considered as the standard control method in industry for this system and has been finally selected as the baseline controller. It should be noticed that the PR controller is also a linear control. Besides, when PR is adopted, a simple PI regulator is usually employed for the outer control loop. Therefore, it is expected that proposed ESO-SOSM provides the same improvements as for the PI-SRF. That is, better transient response and improved system performance under a load step. The performance of the proposed control is compared with a well-tuned conventional PI-SRF controller. The results show that the performance of the designed controller presents a faster dynamic behavior while maintaining a lower THD value in steady state and improves system performance under a load step. The validity of the proposed control algorithm has been verified by experimental results for a 3.0 kVA insulated gate bipolar transistor (IGBT) PWM power converter using a TMS320F28335 digital signal processor (DSP).

The paper is organized as follows: In Section II, the mathematical model for a three-phase two-level grid-connected power converter is presented. Section III shows the design of the proposed SOSM controller for the inner and outer control loops. It also includes the ESO design for estimating the load disturbances. Experimental results comparing the performance of the proposed SOSM control with the conventional PI synchronous reference frame (PI-SRF) controller are discussed in Section IV. Finally, conclusions are drawn in Section V.

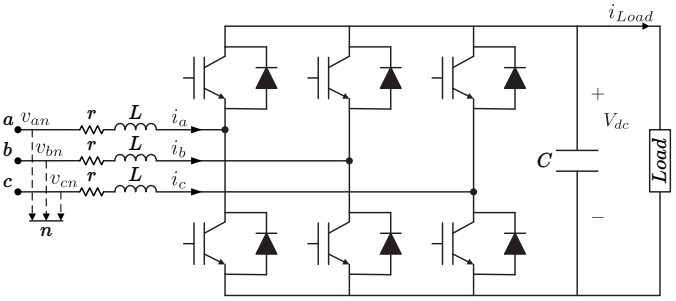

Fig. 1. Circuit of the three-phase two-level grid-connected power converter

II. Problem Formulation

A. Dynamic System Model

The electrical circuit of the three-phase two-level grid-connected power converter under consideration is shown in Fig. 1. The system is connected to the grid through a smoothing inductor L with a parasitic resistance r. It is assumed that an equivalent resistive load R_L is connected at the dc-link capacitor C. The load is considered as an unknown external disturbance.

The grid current and dc-link capacitor voltage dynamics can be written in a dq SRF rotating at the grid frequency [25]. Assuming that grid voltages are balanced then the system model is

$$L\frac{di_d}{dt} = -ri_d + \omega L i_q + v_d - \delta_d V_{dc}, \tag{1}$$

$$L\frac{di_q}{dt} = -ri_q - \omega L i_d + v_q - \delta_q V_{dc}, \tag{2}$$

$$C\frac{dV_{dc}}{dt} = (\delta_d i_d + \delta_q i_q) - i_{Load}, \tag{3}$$

where δ_d, δ_q are the switching functions, v_d, v_q are grid voltages, i_d, i_q are input currents, V_{dc} is dc-link capacitor voltage and ω is the angular frequency of the grid. From the control point of view, working on the dq SRF has the advantage of reducing the current control task into a set-point tracking problem.

It should be pointed out that the amplitude of the control vector is constrained due to the fact that only implementable control vectors are contained in an area limited by the well-known hexagon . Therefore, it is necessary to consider the constraint $\|\delta_{dq}\| \leq \sqrt{2}$, which implies that the switching function stays unsaturated if its magnitude is not larger than $\sqrt{2}$. This is a conservative approach but ensures the system operation.

B. Modelling Uncertainties

In practical applications, the system modeling is usually obtained under several assumptions, e.g. ignore the switching

losses, in order to simplify the control design. However, such models are not exact, and may vary from real system behavior under some operation conditions. Therefore, a controller should be designed to be robust against any modeling parametric uncertainties. For this reason, parametric uncertainties, i.e. smoothing inductor L, parasitic phase resistance r and the angular frequency of the grid ω, are fully considered and included into the model such that the control robustness is guaranteed. These parameters are formalized as follows:

$$L = L_0 + \Delta L,\ r = r_0 + \Delta r,\ \omega = \omega_0 + \Delta\omega, \tag{4}$$

where L_0, r_0, ω_0 are the nominal values and ΔL, Δr, $\Delta\omega$ are the parametric uncertainties which can be considered as unknown slow variant signals.

C. Control Objectives

The control objectives for three-phase two-level grid-connected power converters are as follows:

- The currents i_d, i_q should track their references i_d^* and i_q^*, respectively. The reference value i_d^* is calculated in such a way that dc-link capacitor voltage is regulated to a certain value. The reference value i_q^* is set to provide a desired instantaneous reactive power.

$$i_d \to i_d^*, \quad i_q \to i_q^*. \tag{5}$$

- The dc component of the dc-link capacitor voltage should be driven to some reference value V_{dc}^*.

$$V_{dc} \to V_{dc}^*. \tag{6}$$

III. Control Design

In three-phase two-level grid-connected power converters there exist different kinds of disturbances, like parameter uncertainties and load variations. If the controller does not have enough ability to reject these disturbances then they will degrade the performance of closed loop system. A cascade control structure is used to govern the system (1)-(3). The controller consists of a current tracking loop, inner loop, and an ESO-based voltage regulation loop, outer loop. For the current tracking loop, an STA controller is designed which ensures fast convergence of the currents i_d and i_q to their references i_d^* and i_q^*, respectively. For the voltage regulation loop, an ESO is used to estimate the load power which is considered as an external disturbance. Besides, an STA controller is implemented in parallel to regulate the dc-link capacitor voltage to its desired value using the estimate of the disturbance. First, the basics of STA will be briefly shown. Second, the design of both control loops will be presented.

A. Super-twisting algorithm

The sliding mode design approach consists of two steps. The first step considers the choice of sliding manifold which provides desired performance in the sliding mode. The second step concerns the design of a control law which will force the system states to reach the sliding manifold in finite time, thus the desired performance is attained and maintained. This part discusses the STA in a general case for a single input nonlinear system.

Consider a nonlinear system

$$\dot{x} = a(x) + b(x,u), \tag{7}$$
$$y = s(t,x), \tag{8}$$

where $x \in X \subset \mathcal{R}^n$ is the state vector, $u \in U \subset \mathcal{R}$ is the input, $s(t,x) : \mathcal{R}^{n+1} \to \mathcal{R}$ is the sliding variable and $a(x)$ and $b(x,u)$ are smooth uncertain functions.

The control objective is to force s and its time derivative $\dot{s}$ to zero. By differentiating the sliding variable $s(t,x)$ twice, the following relations are derived:

$$\dot{s} = \frac{\partial}{\partial t}s(t,x) + \frac{\partial}{\partial x}s(t,x)\left[a(x) + b(x,u)\right], \tag{9}$$
$$\begin{aligned}\ddot{s} &= \frac{\partial}{\partial t}\dot{s}(t,x,u) + \frac{\partial}{\partial x}\dot{s}(t,x,u)\left[a(x) + b(x,u)\right] \\ &+ \frac{\partial}{\partial u}\dot{s}(t,x,u)\,\dot{u} \\ &= \varphi(t,x,u) + \gamma(t,x,u)\,\dot{u}.\end{aligned} \tag{10}$$

Assuming that the sliding variable s has relative degree one with respect to the control input u, i.e. $\frac{\partial}{\partial u}\dot{s}(t,x,u) \neq 0$, there exist positive constant values Φ, Γ_m and Γ_M such that the following conditions are satisfied,

$$0 < \Gamma_m < \gamma(t,x,u) < \Gamma_M, \tag{11}$$
$$-\Phi \leq \varphi(t,x,u) \leq \Phi. \tag{12}$$

Under the conditions (11) and (12), the following differential inclusion can be obtained:

$$\ddot{s} \in [-\Phi, +\Phi] + [\Gamma_m, \Gamma_M]\,\dot{u}. \tag{13}$$

In the sequel, a control law based on STA is designed. It consists of two terms, one is the integral of its discontinuous time derivative while the other is a continuous function of the available sliding variable s.

$$u = u_1 + u_2, \tag{14}$$
$$\dot{u}_1 = -\alpha \mathrm{sign}(s), \tag{15}$$
$$u_2 = -\lambda |s|^{\frac{1}{2}} \mathrm{sign}(s), \tag{16}$$

where α and λ are design parameters that can be determined from the boundary conditions (11) and (12). The sufficient conditions for finite time convergence to the sliding manifold $s = \dot{s} = 0$ are [26]:

$$\alpha > \frac{\Phi}{\Gamma_m},\ \lambda^2 \geq \frac{4\Phi}{\Gamma_m^2}\frac{\Gamma_M}{\Gamma_m}\frac{\alpha + \Phi}{\alpha - \Phi}. \tag{17}$$

Remark 1: In the case of relative degree one systems, traditional first order sliding mode could also be applied. However, motivated by the chattering elimination aim, super-twisting based control is employed which means that the control signal u is continuous and chattering is avoided.

B. Extended State Observer

According to the control objective (6), the outer control loop is designed to regulate the output capacitor voltage to its reference value V_{dc}^*.

For the system (1)-(3), the current dynamics are much faster than the dc-link capacitor voltage dynamics [27]. Under this condition, it can be considered that $i_d \cong i_d^*$ and $i_q \cong i_q^*$. Based on the singular perturbation theory [28], if the fast dynamics are stable then (3) will be reduced to

$$C\frac{dV_{dc}}{dt} = \frac{1}{V_{dc}}\left(p^* - p_{load}\right), \tag{18}$$

where $p^* = v_d i_d^* + v_q i_q^*$ and $p_{load} = V_{dc} i_{load}$.

It should be noted from (18) that p_{load} can be considered as an external disturbance. This paper proposes to design an ESO to estimate the disturbance asymptotically. Then, it will be injected into the control design. Unlike traditional observers, such as Luenberger observer [29], high-gain observer [30] and unknown input observer (UIO) [31], ESO regards the disturbances of the system as new system states which are conceived to estimate not only the external disturbances but also plant dynamics [32].

To design the ESO, the new variable $z = V_{dc}^2/2$ is introduced in (18), yielding

$$C\dot{z} = p^* - d(t), \tag{19}$$

with $d(t) = p_{load}$.

A linear ESO is given by

$$C\dot{\hat{z}} = p^* - \hat{d}(t) + \beta_1(z - \hat{z}), \tag{20}$$

$$\dot{\hat{d}}(t) = -\beta_2(z - \hat{z}), \tag{21}$$

where the positive gains β_1 and β_2 are chosen such that the polynomial

$$\lambda^2 + \frac{\beta_1}{C}\lambda + \frac{\beta_2}{C}, \tag{22}$$

is Hurwitz stable. Therefore, its natural frequency ω_n and damping ratio ξ are:

$$\omega_n = \sqrt{\frac{\beta_2}{C}}, \tag{23}$$

$$\xi = \frac{\beta_1}{2}\sqrt{\frac{1}{\beta_2 C}}. \tag{24}$$

Denote the observation errors $\epsilon_z = z - \hat{z}$, $\epsilon_d = d(t) - \hat{d}(t)$, the error dynamics are given by,

$$C\dot{\epsilon}_z = -\beta_1\epsilon_z - \epsilon_d, \tag{25}$$

$$\dot{\epsilon}_d = \beta_2\epsilon_z + h\left(t\right), \tag{26}$$

where $h(t) = \dot{d}(t)$ is the variation rate of load power. The system (25)-(26) can be written as follows:

$$\dot{\epsilon} = A\epsilon + \psi, \tag{27}$$

where $\epsilon = [\epsilon_z,\ \epsilon_d]^T$, $A = \begin{bmatrix} -\frac{\beta_1}{C} & -\frac{1}{C} \\ \beta_2 & 0 \end{bmatrix}$ and $\psi = \begin{bmatrix} 0 & h(t) \end{bmatrix}^T$.

Lemma 1: Suppose that $h\left(t\right)$ is bounded, there exist a constant $\delta > 0$ and a finite time $T_1 > 0$ such that the trajectories of the system (27) are bounded, $\|\epsilon\| \le \delta$, $\forall t \ge T_1 > 0$.

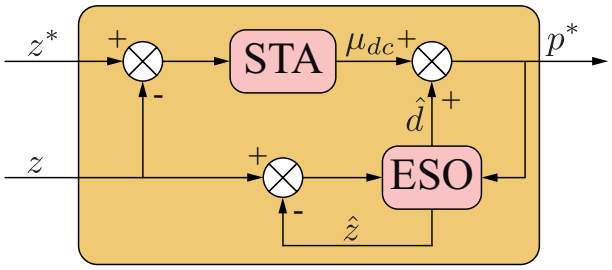

Fig. 2. Block diagram of the STA+ESO controller for the voltage regulation loop

Proof 1: Proof of *Lemma 1* is given in Appendix A.

Remark 2: In view of (25)-(26), the parameters β_1 and β_2 determine the bandwidth of the ESO, i.e.

$$\omega_b = \omega_n\sqrt{(4\xi^4 - 4\xi^2 + 2)}. \tag{28}$$

Generally speaking, the larger the ESO bandwidth is, the more accurate estimation will be achieved. However, this increases the noise sensitivity due to the augment of the bandwidth. The function $h(t)$ represents the rate of change of load power. If this value is quite large then it means that the load power changes very rapidly. In this case, the observer bandwidth needs to be sufficiently large for an accurate estimate of $d(t)$. Therefore, the selection of β_1 and β_2 should balance between the estimation performance and the noise tolerance.

C. Capacitor Voltage Regulation Loop

Define the regulation error $\tilde{z} = z^* - z$ with $z^* = \left(V_{dc}^*\right)^2/2$, it follows that,

$$C\dot{\tilde{z}} = -p^* + d(t). \tag{29}$$

Notice that the perturbation $d(t)$ is an unknown time varying variable. The proposed ESO-based STA controller for the voltage control loop is given by

$$p^* = \mu_{_{dc}}(\tilde{z}) + \hat{d}(t), \tag{30}$$

in which $\mu_{dc}(\tilde{z})$ is the STA which takes the following form,

$$\mu_{dc}(\tilde{z}) = \lambda_{dc}|\tilde{z}|^{\frac{1}{2}}\mathrm{sign}(\tilde{z}) + \alpha_{\mathrm{dc}}\int_0^{\mathrm{t}}\mathrm{sign}(\tilde{z})\mathrm{d}\tau, \tag{31}$$

with some positive constants λ_{dc} and α_{dc}.

Substituting (30) into (29), yields

$$C\dot{\tilde{z}} = -\mu_{dc}(\tilde{z}) + \epsilon_d. \tag{32}$$

It can be easily obtained from the Lemma 1 that

$$\|\dot{\epsilon}_d\| \le \|A\|\,\delta + \sup_{t_0\le\tau\le t}\|\psi\left(\tau\right)\| = F_d, \tag{33}$$

with $\|A\| = \sqrt{\lambda_{\max}(A^TA)}$ and F_d is a positive value. The sufficient conditions for the finite time convergence to the sliding manifold $\tilde{z} = \dot{\tilde{z}} = 0$ are [26]:

$$\alpha_{dc} > CF_d, \quad \lambda_{dc}^2 \ \ge\ 4C^2F_d\frac{\alpha_{dc} + F_d}{\alpha_{dc} - F_d}. \tag{34}$$

The block diagram of the ESO based voltage regulation loop is shown in Fig. 2.

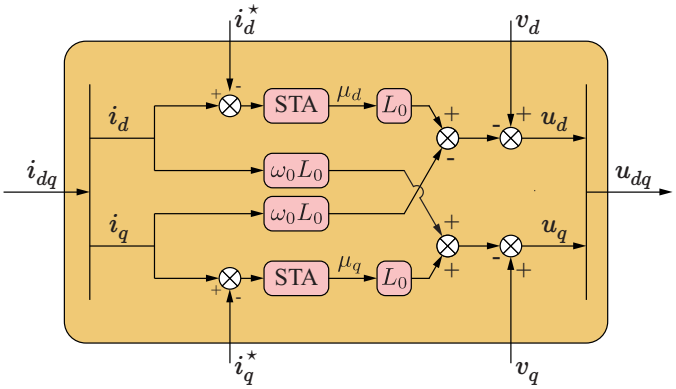

Fig. 3. Block diagram of the current tracking regulation loop

D. Current Tracking Loop

The objective of the inner control loop is to force i_d and i_q to their references i_d^* and i_q^* respectively. The reference current i_d^* is computed from the output of the outer control loop and is calculated to achieve dynamic voltage regulation. The reference current i_q^* is set to provide a desired instantaneous reactive power q^*. Therefore, the current references are calculated as

$$i_d^* = \frac{p^*}{v_d}, \tag{35}$$

$$i_q^* = \frac{q^*}{v_d}. \tag{36}$$

The sliding mode variables for the current control are defined as,

$$s_d = i_d^* - i_d, \tag{37}$$

$$s_q = i_q^* - i_q. \tag{38}$$

Taking the first time derivative of $s_{dq} = [s_d \ s_q]^T$ yields,

$$\begin{bmatrix} \dot{s}_d \\ \dot{s}_q \end{bmatrix} = \begin{bmatrix} \dot{i}_d^* + \frac{r}{L} i_d - \frac{v_d}{L} - \omega i_q \\ \dot{i}_q^* + \frac{r}{L} i_q - \frac{v_q}{L} + \omega i_d \end{bmatrix} + \frac{V_{dc}}{L} \begin{bmatrix} \delta_d \\ \delta_q \end{bmatrix}. \tag{39}$$

In order to satisfy the saturation constraint, the controllers δ_d and δ_q are designed as follows:

$$\delta_d = \sigma\left(m_d\right), \tag{40}$$

$$\delta_q = \sigma\left(m_d\right), \tag{41}$$

where

$$m_d = \frac{L_0}{V_{dc}}\Big[-\mu_d(s_d) + \frac{v_d}{L_0} - \frac{r_0}{L_0} i_d - \dot{i}_d^* + \omega_0 i_q \Big], \tag{42}$$

$$m_q = \frac{L_0}{V_{dc}}\Big[-\mu_q(s_q) + \frac{v_q}{L_0} - \frac{r_0}{L_0} i_q - \dot{i}_q^* - \omega_0 i_d \Big], \tag{43}$$

$\mu_d(s_d)$ and $\mu_q(s_q)$ are STAs which are in the form

$$\mu_d(s_d) = \lambda_d |s_d|^{\frac{1}{2}} \mathrm{sign(s_d)} + \alpha_d \int_0^t \mathrm{sign(s_d)} d\tau, \tag{44}$$

$$\mu_q(s_q) = \lambda_q |s_q|^{\frac{1}{2}} \mathrm{sign(s_q)} + \alpha_q \int_0^t \mathrm{sign(s_q)} d\tau, \tag{45}$$

with some positive constants $\lambda_i, \ \alpha_i, \ i \in \{d, q\}$ and $\sigma(x)$ is a saturation function.

TABLE I
ELECTRICAL SYSTEM PARAMETERS

Parameter	Description
Phase-to-neutral voltage (RMS)	230 V
Grid frequency ω_0	50 Hz
Filter inductor L_0	15 mH
dc-link capacitor C	2800 μF
dc-link voltage reference V_{dc}^*	750 V
sampling frequency f_s	10 kHz
switching frequency f_{sw}	10 kHz

Theorem 1: Consider the system (1)-(3) in closed loop with the saturated controller (40)-(41). This yields

$$\dot{s}_d = -\frac{L_0}{L}\mu(s_d) + \varphi_d(t), \tag{46}$$

$$\dot{s}_q = -\frac{L_0}{L}\mu(s_q) + \varphi_q(t), \tag{47}$$

where

$$\varphi_d(t) = \frac{\Delta r}{L} i_d + \frac{\Delta L}{L} \dot{i}_d^* + \frac{\omega_0 L_0 - \omega L}{L} i_q \tag{48}$$

$$\varphi_q(t) = \frac{\Delta r}{L} i_q + \frac{\Delta L}{L} \dot{i}_q^* - \frac{\omega_0 L_0 - \omega L}{L} i_d. \tag{49}$$

The state trajectories of the system (46)-(47) converge to the origin $s_d = 0, \ s_q = 0$ in finite time if the gains of $\mu(s_d), \ \mu(s_q)$ and V_{dc}^* are chosen such that the following conditions are satisfied,

$$\begin{aligned} \alpha_d &> \frac{\gamma_d}{1-\gamma_0}, \ \lambda_d^2 > \alpha_d, \\ \alpha_q &> \frac{\gamma_q}{1-\gamma_0}, \ \lambda_q^2 > \alpha_q, \end{aligned} \tag{50}$$

and

$$V_{dc}^* > \sqrt{2\left(L\omega \|i_{dq}^*\|\right)^2 + 3E^2}, \tag{51}$$

where γ_0, γ_d and γ_q are positive constants and E is the amplitude of the grid source.

Proof 2: Proof of *Theorem 1* is given in Appendix B.

Remark 3: It should be noted that the cross-coupling terms and the source voltage are compensated by (40)-(43). However, (42)-(43) require the information of the derivative of i_d^* and i_q^*. Usually, these values are zero during the steady state and only affect slightly the system performance during the transient state. Therefore, these terms are neglected in the final control law. Similarly, parameter r_0 is very small in order to reduce system losses. Moreover, this parameter is usually unknown and its use it is also avoided. Taking into account these considerations, the block diagram for the current tracking control loop is shown in Fig. 3, where $u_{dq} = V_{dc}\delta_{dq}$.

IV. EXPERIMENTAL RESULTS

In order to demonstrate the feasibility of the proposed control algorithm, practical results have been performed, comparing the proposed ESO-based SOSM control to a well tuned linear conventional PI-SRF regulator. The PI-SRF is considered as the standard control method for this system

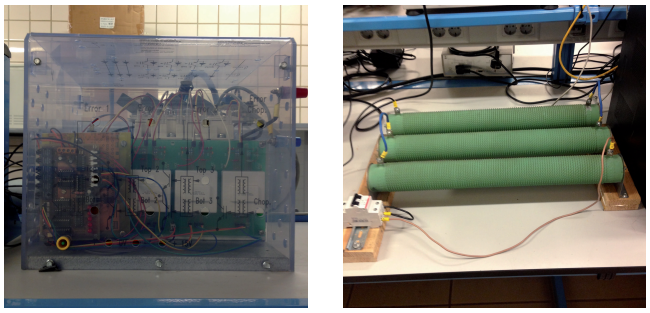

(a) (b)

Fig. 4. Power converter prototype: (a) Power converter, (b) DC load.

TABLE II
CONTROLLER DESIGN PARAMETERS

PI-SRF	Values
Voltage regulation loop ($k_{pdc},\ k_{idc}$)	0.04, 0.5
Current tracking loop ($k_{pd},\ k_{pq},\ k_{id},\ k_{iq}$)	75, 400, 75, 400
ESO-SOSM	**Values**
Voltage regulation loop ($\lambda_{dc},\ \alpha_{dc},\ \beta_1,\ \beta_2$)	3, 750, 3, 300
Current tracking loop ($\lambda_d,\ \alpha_d,\ \lambda_q,\ \alpha_q$)	85, 20000, 85, 20000

and has been selected as a baseline controller. The electrical parameters of the power converter, dc-link voltage reference, and switching and sampling frequencies for the experimental setup are summarized in Table I.

The power converter prototype used for the experiment is shown in Fig. 4. A digital implementation of both current and dc-link voltage control algorithms is executed in a TMS320F28335 floating point digital signal processor board. Two sets of experiments are done. The first one consists of a load step at dc-link from no load to full load (3.125 kW). To perform the experiment, the capacitor voltage reference is set to 750 V and a 180 Ω resistive load is suddenly connected to the dc-link. The second test focuses on the reactive power tracking ability. For this purpose, an instantaneous reactive power command step is done. Measurements of dc-link voltage, phase voltages and currents, harmonic contents of currents, active power, reactive power, and power factor have been taken.

The parameters of the PI-SRF and ESO-SOSM controllers are given in Table II. They are chosen so that the current dynamics are much faster than the capacitor output voltage dynamics. It should be noticed that a Phase Locked Loop (PLL) is also implemented in the digital platform in order to work in the SRF [33].

A. Load Step at DC-Link

The first test consists of evaluating the proposed controller performance under a load step at the dc-link capacitor. Fig. 5 shows the transient response of the dc-link capacitor voltage for a load step from no load to a load composed by a resistor of 180 Ω. Three waveforms are presented. Fig. 5a corresponds with the conventional approach with a PI-SRF controller. Fig. 5b is the result achieved with the proposed

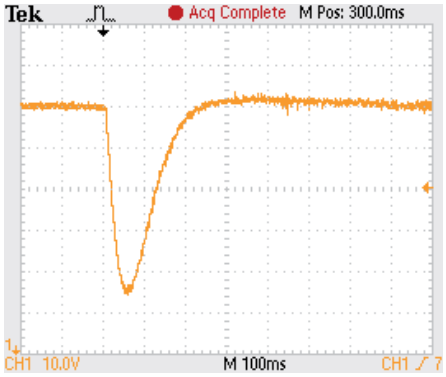

(a)

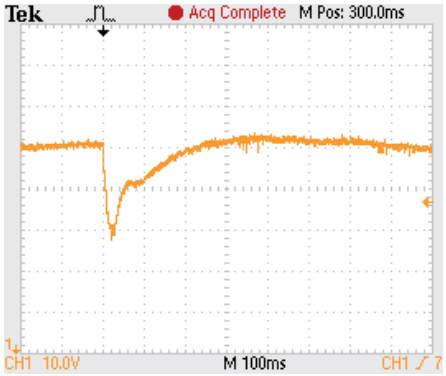

(b)

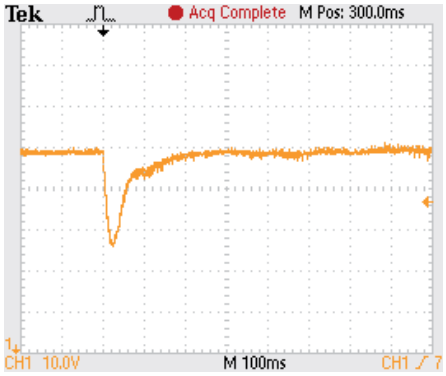

(c)

Fig. 5. Transient response of dc-link capacitor voltage under a load step: (a) PI-SRF algorithm, (b) ESO-SOSM strategy, (c) PI-SRF algorithm with increased bandwidth.

ESO-SOSM algorithm and Fig. 5c is associated to the PI-SRF but increasing the bandwidth of the controller.

Both control laws can achieve the dc-link capacitor voltage regulation. Comparing Fig. 5a with Fig. 5b, the settling time is roughly the same when PI-SRF and ESO-SOSM are used but the last one reduces the dc-link capacitor voltage drop. The PI-SRF results in a voltage drop of 45 V while in the case of the ESO-SOSM approach this is only 22 V. Therefore, the proposed controller reduces the dc-link capacitor voltage drop under a load step in 48.9 %. Clearly the ESO-SOSM requires less energy from the dc-link capacitors compared with the PI-SRF. Same dc-link voltage drop can be achieved with the PI-SRF but it is necessary to increase the outer controller bandwidth. It is possible to do this, but it is well known

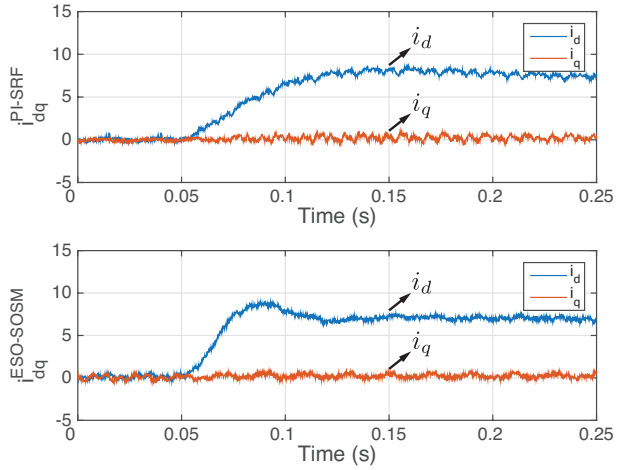

Fig. 6. Transient response of grid currents in the dq frame under a load step. Top: PI-SRF algorithm. Bottom: ESO-SOSM strategy.

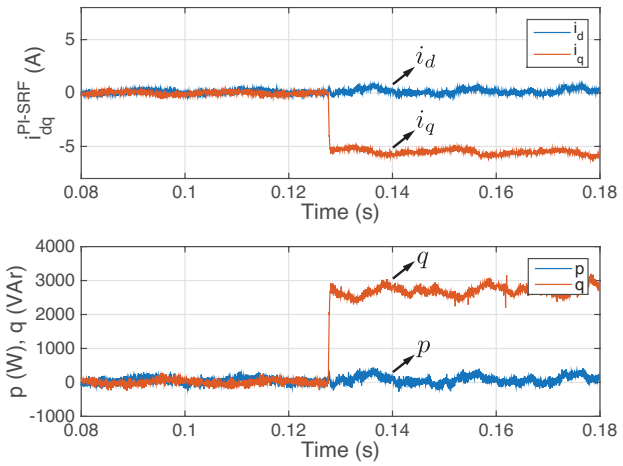

Fig. 7. Transient response of grid currents in the dq frame under a load step for the PI-SRF algorithm. Top: Grid currents in the SRF. Bottom: Instantaneous active and reactive power.

TABLE III
GRID CURRENT THD FOR THE LOAD STEP EXPERIMENT

Controller	THD(%)
PI-SRF	2.4
ESO-SOSM	2.1
PI-SRF $((k_{pdc}, k_{idc}) * 3)$	4.9

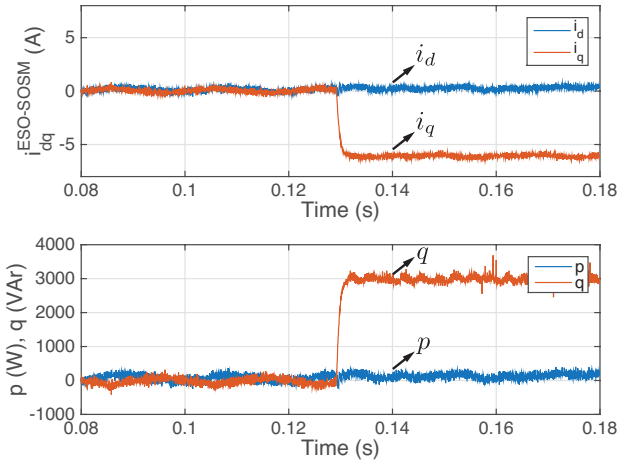

Fig. 8. Transient response of grid currents in the dq frame under a load step for the ESO-SOSM strategy. Top: Grid currents in the SRF. Bottom: Instantaneous active and reactive power.

that increasing the bandwidth of the outer control loop in the conventional PI-SRF affects the grid current harmonic content. Table III collects the current THD computed up to 50^{th} harmonics for the three situations. Clearly the ESO-SOSM allows to achieve a better transient response while maintaining a low THD in steady state.

Fig. 6 plots the grid currents for the load step at the dc-link capacitor tests. The waveforms are represented in the SRF. Only the currents for Fig. 5a and Fig. 5b are plotted. Clearly the PI-SRF presents a slow transient response and needs some time to reach the steady state value. On the other hand, the ESO-SOSM approach quickly changes the i_d current component value. It should be noticed that i_d^* comes from the outer control loop. Therefore, the ESO introduced in the control law provides a clear improvement compared with the conventional approach that only considers a PI for the dc-link voltage regulation.

B. Reactive Power Command Step

The second experiment assesses the control law capability to provide a desired amount of reactive power. To do so, it is introduced a instantaneous reactive power command step from 0 to 3 kVAr. The system response is evaluated for both the PI-SRF and ESO-SOSM controllers.

Fig. 7 presents the transient state for the experimental results achieved by the PI-SRF and Fig. 8 shows the corresponding one to the ESO-SOSM. As expected, both controllers provide the desired reactive power. However, the dynamic response for the ESO-SOSM is faster than the PI-SRF. Most interesting is the steady state behavior. Fig. 9a-Fig. 9c show the steady state features for the PI-SRF controller. Fig. 9a, Fig. 9b and Fig. 9c are the grid currents, the current spectrum and information about the active power, reactive power values and the power factor respectively. On the other hand Fig. 9e-Fig. 9f present the same information in the case of the ESO-SOSM approach. Comparing the grid spectrum in Fig. 9b and Fig. 9e the ESO-SOSM controller has better performance. Particularly, the 5^{th} and 7^{th} harmonics are reduced compared with the PI-SRF results. Furthermore, the current THD is 1.2 % for the ESO-SOSM and 1.7 % for the PI-SRF. This supposes a reduction of 29.4 % when the ESO-SOSM approach is used in the same power converter prototype.

V. CONCLUSION

Second order sliding mode (SOSM) technique is a promising alternative for the control of three-phase two-level grid-

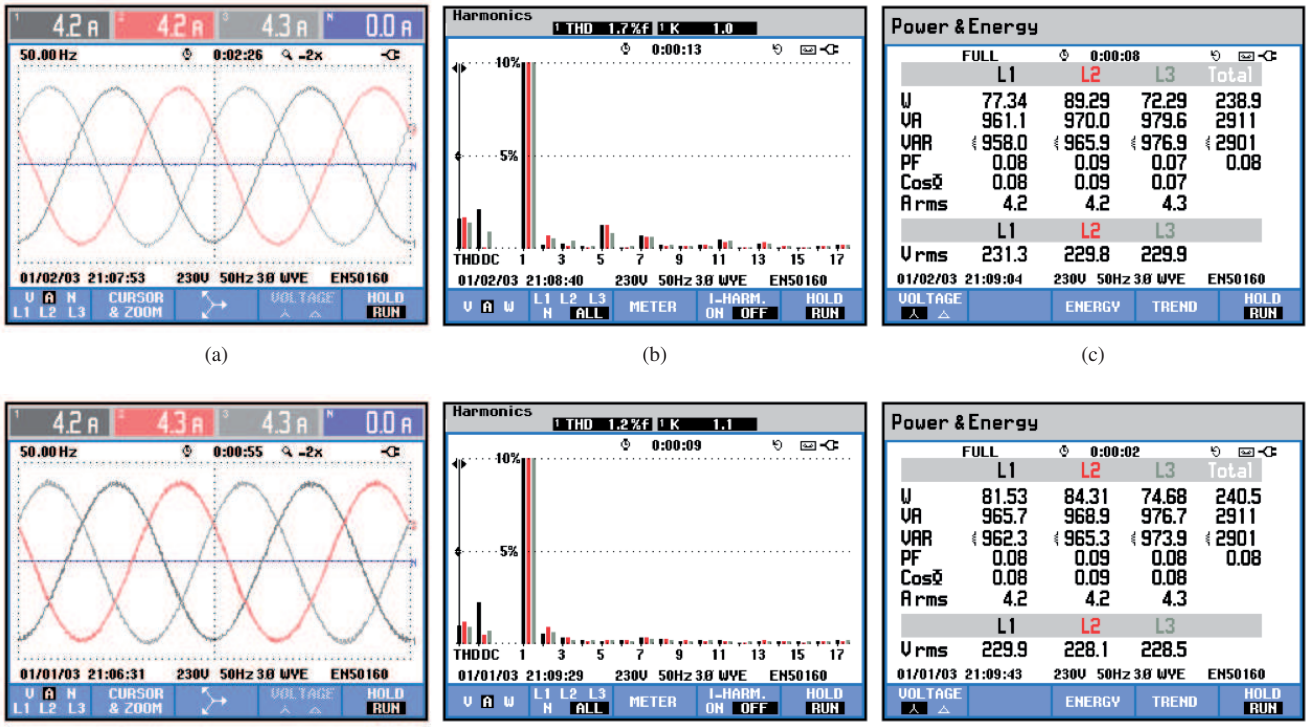

(a) (b) (c)

(d) (e) (f)

Fig. 9. Steady state currents for a instantaneous reactive power command of 3 kVAr: (a) Current waveforms for PI-SRF algorithm, (b) Current spectrum for PI-SRF algorithm, (c) Power factor for PI-SRF algorithm, (d) Current waveforms for ESO-SOSM strategy, (e) Current spectrum for ESO-SOSM algorithm, (f) Power factor for ESO-SOSM strategy.

connected power converters due to its features of robustness and effectiveness for nonlinear systems. Considering the dynamics of the output voltage, the load connected to the dc-link capacitor is regarded as a disturbance for the voltage control loop, which directly affects the performance of the whole system. To improve the disturbance rejection ability, a composite control law consisting of SOSM based on super twisting algorithm (STA) and disturbance compensation via extended state observer (ESO) is proposed for the voltage regulation loop. With the disturbance compensation using ESO, the gains of STA for the outer control loop can be reduced without decreasing the settling time and reducing the dc-link capacitor voltage drop. The current loop has been designed to track the current references in the presence of system parameter uncertainties using an STA. Experimental results have demonstrated that the proposed ESO-SOSM controller performs better than that of the the conventional PI SRF control. The power converter operated with the proposed algorithm has achieved less dc-link voltage drop under a sudden load step, shorter settling time and better grid current quality in terms of lower THD and reduced values of low-order harmonics content.

APPENDIX

A. Proof of Lemma 1

Solving (27), one has

$$\epsilon(t) = e^{(t-t_0)A}\epsilon(t_0) + \int_{t_0}^{t} e^{(t-\tau)A}\psi(\tau)\,d\tau, \qquad (52)$$

where t_0 is the initial time. Using the bound $\left\|e^{(t-t_0)A}\right\| \leq ke^{-\beta(t-t_0)}$, with $k>0$, $\beta>0$, then (52) can be estimated as follows:

$$\begin{aligned}\|\epsilon(t)\| &\leq ke^{-\beta(t-t_0)}\|\epsilon(t_0)\| + \int_{t_0}^{t} ke^{-\beta(t-\tau)}\|\psi(\tau)\|\,d\tau \\ &\leq ke^{-\beta(t-t_0)}\|\epsilon(t_0)\| + \frac{k}{\beta}\sup_{t_0\leq\tau\leq t}\|\psi(\tau)\|. \qquad (53)\end{aligned}$$

It follows from (53) that $\|\epsilon\| \leq \delta$, $\forall t \geq T_1 > 0$, where δ is a positive constant that depends on k, β and the upper bound of $\|\psi(\tau)\|$.

B. Proof of Theorem 1

The proof is divided into two parts. Firstly, if the control vector $\|\delta_{dq}\| \leq \sqrt{2}$, then $\delta_{dq} = [m_d,\ m_q]^T$. Secondly, in the case when the control vector $\|u_{dq}\| > \sqrt{2}$, thus the control vector is saturated to that value.

Case 1: The controller is given by $\delta_d = m_d$ and $\delta_q = m_q$ in (40)-(41). Considering closed loop behavior (46)-(47) and given that (1)-(3) is a physical system, thus it is reasonable to assume that the variables $\varphi_d(t)$ and $\varphi_q(t)$ and its time derivatives are bounded functions:

$$\|\dot{\varphi}_d(t)\| \leq \gamma_d, \quad \|\dot{\varphi}_q(t)\| \leq \gamma_q, \qquad (54)$$

with some positive constants γ_d and γ_q. Taking into account that

$$(1-\gamma_0)L \leq L_0 \leq (1+\gamma_0)L, \qquad (55)$$

for some scalar $0 < \gamma_0 < 1$. Then, according to [26], the trajectories of the system (46)-(47) will converge to $s_d = \dot{s}_d = 0$ and $s_q = \dot{s}_q = 0$ in finite time when the controller gains satisfy conditions (50).

Case 2: According to [34], the sufficient condition for the control vector δ_{dq} to enter into the circle of radium $\sqrt{2}$, (i.e., $\|\delta_{dq}\| \leq \sqrt{2}$) is that V_{dc}^* satisfies the condition (51). Thus, Theorem 1 is proven.

REFERENCES

[1] J. M. Carrasco, L. G. Franquelo, J. T. Bialasiewicz, E. Galvan, R. C. P. Guisado, M. A. M. Prats, J. I. Leon, and N. Moreno-Alfonso, "Power-electronic systems for the grid integration of renewable energy sources: A survey," *IEEE Trans. Ind. Electron.*, vol. 53, DOI 10.1109/TIE.2006.878356, no. 4, pp. 1002–1016, Jun. 2006.

[2] E. Romero-Cadaval, G. Spagnuolo, L. G. Franquelo, C. A. Ramos-Paja, T. Suntio, and W. M. Xiao, "Grid-connected photovoltaic generation plants: Components and operation," *IEEE Ind. Electron. Mag.*, vol. 7, DOI 10.1109/MIE.2013.2264540, no. 3, pp. 6–20, Sep. 2013.

[3] S. Kouro, J. I. Leon, D. Vinnikov, and L. G. Franquelo, "Grid-connected photovoltaic systems: An overview of recent research and emerging pv converter technology," *IEEE Ind. Electron. Mag.*, vol. 9, DOI 10.1109/MIE.2014.2376976, no. 1, pp. 47–61, Mar. 2015.

[4] S. Vazquez, S. M. Lukic, E. Galvan, L. G. Franquelo, and J. M. Carrasco, "Energy storage systems for transport and grid applications," *IEEE Trans. Ind. Electron.*, vol. 57, DOI 10.1109/TIE.2010.2076414, no. 12, pp. 3881–3895, Dec. 2010.

[5] M. P. Kazmierkowski, L. G. Franquelo, J. Rodriguez, M. A. Perez, and J. I. Leon, "High-performance motor drives," *IEEE Ind. Electron. Mag.*, vol. 5, DOI 10.1109/MIE.2011.942173, no. 3, pp. 6–26, Sep. 2011.

[6] S. Vazquez, A. Marquez, R. Aguilera, D. Quevedo, J. I. Leon, and L. G. Franquelo, "Predictive optimal switching sequence direct power control for grid-connected power converters," *IEEE Trans. Ind. Electron.*, vol. 62, DOI 10.1109/TIE.2014.2351378, no. 4, pp. 2010–2020, Apr. 2015.

[7] C. T. Pan and T. C. Chen, "Modelling and analysis of a three phase pwm ac-dc convertor without current sensor," *IEE Proceedings B - Electric Power Applications*, vol. 140, DOI 10.1049/ip-b.1993.0024, no. 3, pp. 201–208, May. 1993.

[8] R. Wu, S. B. Dewan, and G. R. Slemon, "A pwm ac-to-dc converter with fixed switching frequency," *IEEE Trans. Ind. Appl.*, vol. 26, DOI 10.1109/28.60060, no. 5, pp. 880–885, Sep. 1990.

[9] J. Linares-Flores, A. H. Mendez, C. Garcia-Rodriguez, and H. Sira-Ramirez, "Robust nonlinear adaptive control of a boost converter via algebraic parameter identification," *IEEE Trans. Ind. Electron.*, vol. 61, DOI 10.1109/TIE.2013.2284150, no. 8, pp. 4105–4114, Aug. 2014.

[10] L. Harnefors, A. G. Yepes, A. Vidal, and J. Doval-Gandoy, "Passivity-based controller design of grid-connected vscs for prevention of electrical resonance instability," *IEEE Trans. Ind. Electron.*, vol. 62, DOI 10.1109/TIE.2014.2336632, no. 2, pp. 702–710, Feb. 2015.

[11] S. Vazquez, J. I. Leon, L. G. Franquelo, J. Rodriguez, H. A. Young, A. Marquez, and P. Zanchetta, "Model predictive control: A review of its applications in power electronics," *IEEE Ind. Electron. Mag.*, vol. 8, DOI 10.1109/MIE.2013.2290138, no. 1, pp. 16–31, Mar. 2014.

[12] J. F. Silva, "Sliding-mode control of boost-type unity-power-factor pwm rectifiers," *IEEE Trans. Ind. Electron.*, vol. 46, DOI 10.1109/41.767067, no. 3, pp. 594–603, Jun. 1999.

[13] D. M. Vilathgamuwa, S. R. Wall, and R. D. Jackson, "Variable structure control of voltage sourced reversible rectifiers," *IEE Proceedings - Electric Power Applications*, vol. 143, DOI 10.1049/ip-epa:19960039, no. 1, pp. 18–24, Jan. 1996.

[14] S. C. Tan, Y. M. Lai, C. K. Tse, L. Martinez-Salamero, and C. K. Wu, "A fast-response sliding-mode controller for boost-type converters with a wide range of operating conditions," *IEEE Trans. Ind. Electron.*, vol. 54, DOI 10.1109/TIE.2007.905969, no. 6, pp. 3276–3286, Dec. 2007.

[15] Y. Shtessel, S. Baev, and H. Biglari, "Unity power factor control in three-phase ac/dc boost converter using sliding modes," *IEEE Trans. Ind. Electron.*, vol. 55, DOI 10.1109/TIE.2008.2003203, no. 11, pp. 3874–3882, Nov. 2008.

[16] J. Liu, S. Laghrouche, and M. Wack, "Observer-based higher order sliding mode control of power factor in three-phase ac/dc converter for hybrid electric vehicle applications," *International Journal of Control*, vol. 87, no. 6, pp. 1117–1130, 2014.

[17] W. Gao and J. C. Hung, "Variable structure control of nonlinear systems: a new approach," *IEEE Trans. Ind. Electron.*, vol. 40, DOI 10.1109/41.184820, no. 1, pp. 45–55, Feb. 1993.

[18] A. Levant, "Higher-order sliding modes, differentiation and output-feedback control," *International Journal of Control*, vol. 76, no. 9-10, pp. 924–941, 2003.

[19] J. Y. Hung, W. Gao, and J. C. Hung, "Variable structure control: a survey," *IEEE Trans. Ind. Electron.*, vol. 40, DOI 10.1109/41.184817, no. 1, pp. 2–22, Feb. 1993.

[20] S. Yin, H. Yang, H. Gao, J. Qiu, and O. Kaynak, "An adaptive nn-based approach for fault-tolerant control of nonlinear time-varying delay systems with unmodeled dynamics," *IEEE Trans. Neural Netw. Learn. Syst.*, vol. PP, DOI 10.1109/TNNLS.2016.2558195, no. 99, pp. 1–12, 2016.

[21] S. Yin, H. Gao, J. Qiu, and O. Kaynak, "Adaptive fault-tolerant control for nonlinear system with unknown control directions based on fuzzy approximation," *IEEE Trans. Syst., Man, Cybern., Syst.*, vol. PP, DOI 10.1109/TSMC.2016.2564921, no. 99, pp. 1–10, 2016.

[22] J. Liu, S. Vazquez, H. Gao, and L. G. Franquelo, "Robust control for three-phase grid connected power converters via second order sliding mode," in *Industrial Technology (ICIT), 2015 IEEE International Conference on*, DOI 10.1109/ICIT.2015.7125252, Mar. 2015, pp. 1149–1154.

[23] S. Vazquez, J. Liu, H. Gao, and L. G. Franquelo, "Second order sliding mode control for three-level npc converters via extended state observer," in *Industrial Electronics Society, IECON 2015 - 41st Annual Conference of the IEEE*, DOI 10.1109/IECON.2015.7392903, Nov. 2015, pp. 005 118–005 123.

[24] T. Gonzalez, J. A. Moreno, and L. Fridman, "Variable gain super-twisting sliding mode control," *IEEE Trans. Autom. Control*, vol. 57, DOI 10.1109/TAC.2011.2179878, no. 8, pp. 2100–2105, Aug. 2012.

[25] V. Blasko and V. Kaura, "A new mathematical model and control of a three-phase ac-dc voltage source converter," *IEEE Trans. Power Electron.*, vol. 12, DOI 10.1109/63.554176, no. 1, pp. 116–123, Jan. 1997.

[26] A. Levant, "Sliding order and sliding accuracy in sliding mode control," *International Journal of Control*, vol. 58, no. 6, pp. 1247–1263, 1993.

[27] F. Umbria, J. Aracil, F. Gordillo, F. Salas, and J. A. Sanchez, "Three-time-scale singular perturbation stability analysis of three-phase power converters," *Asian Journal of Control*, vol. 16, no. 5, pp. 1361–1372, 2014.

[28] H. K. Khalil, *Nonlinear Systems*, 3rd ed. Prentice Hall, 2001.

[29] D. G. Luenberger, "Observing the state of a linear system," *IEEE Trans. Mil. Electron.*, vol. 8, DOI 10.1109/TME.1964.4323124, no. 2, pp. 74–80, Apr. 1964.

[30] A. N. Atassi and H. K. Khalil, "A separation principle for the stabilization of a class of nonlinear systems," *IEEE Trans. Autom. Control*, vol. 44, DOI 10.1109/9.788534, no. 9, pp. 1672–1687, Sep. 1999.

[31] M.-S. Chen and C.-C. Chen, "Unknown input observer for linear non-minimum phase systems," *Journal of the Franklin Institute*, vol. 347, no. 2, pp. 577 – 588, 2010.

[32] J. Han, "From pid to active disturbance rejection control," *IEEE Trans. Ind. Electron.*, vol. 56, DOI 10.1109/TIE.2008.2011621, no. 3, pp. 900–906, Mar. 2009.

[33] S. Vazquez, J. A. Sanchez, M. R. Reyes, J. I. Leon, and J. M. Carrasco, "Adaptive vectorial filter for grid synchronization of power converters under unbalanced and/or distorted grid conditions," *IEEE Trans. Ind. Electron.*, vol. 61, DOI 10.1109/TIE.2013.2258302, no. 3, pp. 1355–1367, Mar. 2014.

[34] G. Escobar, R. Ortega, and A. J. Van der Schaft, "A saturated output feedback controller for the three phase voltage sourced reversible boost type rectifier," in *Industrial Electronics Society, 1998. IECON '98. Proceedings of the 24th Annual Conference of the IEEE*, vol. 2, DOI 10.1109/IECON.1998.724176, Aug. 1998, pp. 685–690 vol.2.

Jianxing Liu (M'13) received the B.S. degree in mechanical engineering in 2004, the M.E. degree in control science and engineering in 2010, both from Harbin Institute of Technology, Harbin, China and the PhD degree in automation from the Technical University of Belfort-Montbeliard (UTBM), France, in 2014. Since 2014, he is with Harbin Institute of Technology, China. His current research interests include sliding mode control, nonlinear control and observation, industrial electronics and renewable energy solutions.

Sergio Vazquez (S'04, M'08, SM'14) was born in Seville, Spain, in 1974. He received the M.S. and PhD degrees in industrial engineering from the University of Seville (US) in 2006, and 2010, respectively. Since 2002, he is with the Power Electronics Group working in R&D projects. He is an Associate Professor with the Department of Electronic Engineering, US. His research interests include power electronics systems, modeling, modulation and control of power electronics converters applied to renewable energy technologies. Dr. Vazquez was recipient as coauthor of the 2012 Best Paper Award of the IEEE Transactions on Industrial Electronics and 2015 Best Paper Award of the IEEE Industrial Electronics Magazine. He is involved in the Energy Storage Technical Commiteee of the IEEE industrial electronics society and is currently serving as an Associate Editor of the IEEE Transactions on Industrial Electronics.

Ligang Wu (M'10-SM'12) received the B.S. degree in Automation from Harbin University of Science and Technology, China in 2001; the M.E. degree in Navigation Guidance and Control from Harbin Institute of Technology, China in 2003; the PhD degree in Control Theory and Control Engineering from Harbin Institute of Technology, China in 2006. From January 2006 to April 2007, he was a Research Associate in the Department of Mechanical Engineering, The University of Hong Kong. From September 2007 to June 2008, he was a Senior Research Associate in City University of Hong Kong. From December 2012 to December 2013, he was a Research Associate in Imperial College London, UK. In 2008, he joined the Harbin Institute of Technology, China, as an Associate Professor, and was then promoted to a Professor in 2012. Dr. Wu was the winner of the National Science Fund for Distinguished Young Scholars in 2015. He received China Young Five Four Medal in 2016. Dr. Wu currently serves as an Associate Editor for a number of IEEE journals. His current research interests include switched systems, stochastic systems, computational and intelligent systems, multidimensional systems, sliding mode control, and flight control.

Abraham Marquez (M'15) was born in Huelva, Spain, in 1985. He received his B.Eng. degree in telecommunications engineering from the University of Seville (US), Spain, in 2014. He was granted a scholarship from the Asociación de Investigación y Cooperación Industrial de Andalucía to pursue his M.S. degree in power electronics at US. His main research interest is the model-based predictive control of power converters and drives. Mr. Marquez was recipient as coauthor of the 2015 Best Paper Award of the IEEE Industrial Electronics Magazine.

Huijun Gao (SM'09, F'14) received the Ph.D. degree in control science and engineering from the Harbin Institute of Technology, Harbin, China, in 2005. From 2005 to 2007, he conducted his postdoctoral research with the Department of Electrical and Computer Engineering, University of Alberta, Edmonton, AB, Canada. Since 2004, he has been with the Harbin Institute of Technology, where he is currently a Professor and the Director of the Research Institute of Intelligent Control and Systems. His current research interests include network-based control, robust control/filter theory, and time-delay systems and their engineering applications. He is the Co-Editor-in-Chief of the IEEE TRANSACTIONS ON INDUSTRIAL ELECTRONICS and an Associate Editor of Automatica, the IEEE TRANSACTIONS ON CYBERNETICS, the IEEE TRANSACTIONS ON FUZZY SYSTEMS, the IEEE/ASME TRANSACTIONS ON MECHATRONICS, and the IEEE TRANSACTIONS ON CONTROL SYSTEMS TECHNOLOGY. He is an Administrative Committee Member of the IEEE Industrial Electronics Society.

Leopoldo G. Franquelo (M'84-SM'96-F'05) was born in Malaga, Spain. He received the M.Sc. and Ph.D. degrees in electrical engineering from the Universidad de Sevilla, Seville, Spain in 1977 and 1980 respectively. Dr. Franquelo has been a Industrial Electronics Society (IES) Distinguished Lecturer since 2006, an Associate Editor for the IEEE Transactions on Industrial Electronics since 2007, Co-Editor-in-Chief since 2014, and Editor-in-Chief since 2015. He was a Member-at-Large of the IES AdCom (2002-2003), the Vice President for Conferences (2004-2007), and the President Elect of the IES (2008-2009). He was the President of the IEEE Industrial Electronics Society (2010-2011) and currently is IES AdCom Life member. His current research interest lies on modulation techniques for multilevel inverters and its application to power electronic systems for renewable energy systems. He has received a number of best paper awards from journals of the IEEE. In 2012 and 2015 he received the Eugene Mittelmann Award and the Antohny J. Hornfeck Service Award from IES respectively